Chemistry–A European Journal
Research Article
doi.org/10.1002/chem.202301159
Chemistry Europe
European Chemical Societies Publishing
www.chemeurj.org

Hot Paper

Fibrils Emerging from Droplets: Molecular Guiding Principles behind Phase Transitions of a Short Peptide-Based Condensate Studied by Solid-State NMR**

Wojciech P. Lipiński[+],[a] Johannes Zehnder[+],[b] Manzar Abbas,[a] Peter Güntert,[b, c, d] Evan Spruijt[+],*[a] and Thomas Wiegand[+]*[e, f]

Biochemical reactions occurring in highly crowded cellular environments require different means of control to ensure productivity and specificity. Compartmentalization of reagents by liquid-liquid phase separation is one of these means. However, extremely high local protein concentrations of up to 400 mg/ml can result in pathological aggregation into fibrillar amyloid structures, a phenomenon that has been linked to various neurodegenerative diseases. Despite its relevance, the process of liquid-to-solid transition inside condensates is still not well understood at the molecular level. We thus herein use small peptide derivatives that can undergo both liquid-liquid and subsequent liquid-to-solid phase transition as model systems to study both processes. Using solid-state nuclear magnetic resonance (NMR) and transmission electron microscopy (TEM), we compare the structure of condensed states of leucine, tryptophan and phenylalanine containing derivatives, distinguishing between liquid-like condensates, amorphous aggregates and fibrils, respectively. A structural model for the fibrils formed by the phenylalanine derivative was obtained by an NMR-based structure calculation. The fibrils are stabilised by hydrogen bonds and side-chain π-π interactions, which are likely much less pronounced or absent in the liquid and amorphous state. Such noncovalent interactions are equally important for the liquid-to-solid transition of proteins, particularly those related to neurodegenerative diseases.

Introduction

Many different proteins have recently been shown to participate in liquid-liquid phase separation (LLPS), both in vitro and in vivo. In living cells, liquid condensates, also referred to as membraneless organelles (MLOs), can fulfil various biological functions.[1–4] While MLOs are often recognized for their dynamic state,[5] it has been reported that many protein-based condensates may gradually transform into gel-like or even entirely solid aggregates. In certain cases, such a transition is required for the function of the organelle, for example in Balbiani bodies[6] or in heterochromatin assembly.[7] However, most MLOs depend on a dynamic interior for their natural function, and the appearance of solid or gel-like states has been linked to pathological conditions.[8] Several proteins involved in liquid-to-solid transitions (LST) of MLOs belong to the class of RNA-binding proteins and are linked with neurodegenerative diseases,[9] such as amyotrophic lateral sclerosis (ALS).[10] In addition, mutations in intrinsically disordered regions (IDRs) of proteins that undergo LLPS can accelerate the maturation of initially liquid droplets into gels or solid aggregates. Examples of proteins that can undergo LLPS but that can also form solid-like aggregates include fused in sarcoma (FUS),[11] tau[12] and heterogeneous nuclear ribonucleoprotein A1 (hnRNPA1).[13]

[a] W. P. Lipiński,[+] Dr. M. Abbas, Dr. E. Spruijt[+]
Radboud University
Institute of Molecules and Materials (IMM)
Heyendaalseweg 135, 6525 AJ Nijmegen (the Netherlands)
E-mail: e.spruijt@science.ru.nl

[b] Dr. J. Zehnder,[+] Prof. Dr. P. Güntert
Physical Chemistry
ETH Zurich
Vladimir-Prelog-Weg 2, 8093 Zurich (Switzerland)

[c] Prof. Dr. P. Güntert
Institute of Biophysical Chemistry
Center for Biomolecular Magnetic Resonance
Goethe University Frankfurt am Main
Max-von-Laue-Str. 9, 60438 Frankfurt am Main (Germany)

[d] Prof. Dr. P. Güntert
Department of Chemistry
Tokyo Metropolitan University
1-1 Minamiosawa, Hachioji-shi, 192-0397 Tokyo (Japan)

[e] Prof. Dr. T. Wiegand[+]
Max Planck Institute for Chemical Energy Conversion
Stiftstr. 34–36, 45470 Mülheim an der Ruhr (Germany)
E-mail: thomas.wiegand@cec.mpg.de

[f] Prof. Dr. T. Wiegand[+]
Institute of Technical and Macromolecular Chemistry
RWTH Aachen University
Worringerweg 2, 52074 Aachen (Germany)

[+] These authors have contributed equally.

[**] A previous version of this manuscript has been deposited on a preprint server (https://chemrxiv.org/engage/chemrxiv/article-details/6346cb8c2e6e7c07ca58cbd8).

Supporting information for this article is available on the WWW under https://doi.org/10.1002/chem.202301159

Despite the widespread occurrence of condensate maturation and solidification, it remains elusive how the molecular properties of molecules undergoing LLPS affect the LSTs and the structural characteristics of gel or solid aggregates. Multivalency has been proposed as a requirement for the formation of MLOs through LLPS.[5,14] Weak, noncovalent interactions (e.g., charge-charge, π-π or cation-π interactions, hydrogen bonding, as well as hydrophobic interactions) within IDRs of a protein have been shown to drive LLPS, but these interactions can also promote a self-assembly process into cross-β structures very similar to those observed in amyloid fibrils.[6,11–13,15–18] In recent work, the importance of noncovalent interactions in LLPS has been outlined, and in particular cation-π interactions between tyrosine and positively charged arginine sidechains were identified as possible drivers of both LLPS and assembly into ordered filaments.[19] In solution or in condensates that remain stable as liquid droplets, stretches of polar residues provide enough separation between the (mostly) aromatic residues that are involved in the association to prevent aggregation. This is commonly described as a sticker-and-spacer model.[20] However, we currently lack a molecular understanding of the LST and a structural model of the different states of assembly, since model systems in which the chemical nature and position of stickers and spacers can be readily changed are missing.

Here, we study the behaviour of small synthetic peptide derivatives that are able to undergo LLPS and LST. They represent a minimal model of phase separating proteins based on a sticker-and-spacer motif. We show that these simple derivatives can recapitulate the broad scope of phases found in the IDR-containing proteins, ranging from the formation of stable liquid droplets, maturation and transformation into arrays of ordered solid fibrils, and immediate solid precipitation. Unlike the IDR-containing proteins, this system is sufficiently simple that it allows detailed structural characterization at a level that cannot be achieved for proteins undergoing LST. Despite the recent endeavours to study the condensed protein phase using spectroscopic methods,[21,22] optical methods[23] and simulations,[24] many open questions about protein LLPS and LST still remain, and can be potentially answered using model systems.

Solid-state NMR under magic-angle spinning (MAS) is the method-of-choice to study protein samples in macroscopically condensed phases and has been particularly successful to determine the structures of a variety of amyloid fibrils.[25–30] It has also recently been employed in the context of phase separation.[31–37] A particular strength of NMR is the possibility to distinguish different polymorphs, which are often observed in the context of amyloid fibrils[25,38,39] and may be of relevance in the context of LST. We performed structural solid-state NMR studies, complemented with transmission electron microscopy (TEM), atomic-force microscopy (AFM) and X-ray diffraction, of several model peptide derivatives with an XXssXX motif, in which two dipeptide sticker moieties (XX) are linked together via a flexible disulphide bond. Using specifically $^{13}C/^{15}N$ labelled samples, we derive a structural model for the formed fibril state highlighting the role of intermolecular π-π interactions in phase separation. Better understanding of the molecular structure of the dense liquid and fibril-like states, and of the interactions stabilising both phases, will provide insight also into the pathological transitions of proteins, which is crucial to develop new methods of preventing and curing aggregation-related diseases.

Results and Discussion

Small peptide derivatives are model systems that can undergo phase separation

We have previously described properties of FFssFF (Figure 1a) and similar derivatives.[40] These derivatives are typically soluble in acidic conditions (pH below 6.5), but undergo LLPS above pH 7. Derivatives of dipeptides containing phenylalanine and/or leucine residues and a linker with one or two sulphur atoms, like FFssFF, LLssLL, LFssFL, FLssLF and FFsFF (see Figure S1 for the chemical structures), were all found to undergo LLPS above a characteristic saturation concentration.[40] Derivatives containing tryptophan residues (WWssWW) formed solid aggregates directly from solution at room temperature (Figure 1b). We have previously shown that the condensates formed by FFssFF and other derivatives have characteristics of coacervates: they form spherical droplets containing 50–70% (w/w) water that undergo fusion, wet the glass surface, and recover after photobleaching, while aggregates formed by WWssWW are not dynamic and show no recovery. These findings could be rationalized in terms of the relative hydrophobicity of the sticker residues that underlie LLPS: when the interaction between stickers is too strong, stacking interactions and limited backbone flexibility in derivatives containing tryptophan residues prevent a dynamic exchange inside condensates, and result in an arrested, solid-like state.

Interestingly, we observed that the liquid droplets formed by derivatives with phenylalanine (and mixed F and L) could undergo a LST upon incubation at elevated temperatures. We also observed that this transition can be induced by mechanical shear, similarly to LST described more generally for proteins and peptides undergoing LLPS.[41] LST of our peptide derivatives typically occurred within 2–5 h when concentrated samples (10 mg/ml) were agitated during incubation at 37 °C. In optical microscopy images, this is manifested by condensates that acquired irregular shapes (the average circularity decreased) and show non-homogenous light transmission (Figure S2). TEM of samples collected at different incubation times show a gradual transition from homogenous, droplet-like condensates into fibrils (Figure 1c). The TEM images suggest that fibril formation is nucleated inside the droplets or at their interface, the latter has been reported for instance very recently in the context of the hnRNPA1 protein.[42]

Investigation by TEM shows that all solid aggregates formed through LST have a fibrilar structure, although the fibrils appear to have different morphology for different derivatives (Figure 1d). This is in contrast to solid aggregates that form upon immediate precipitation from solution by WWssWW, as these aggregates appear amorphous. Interestingly, the appearance of

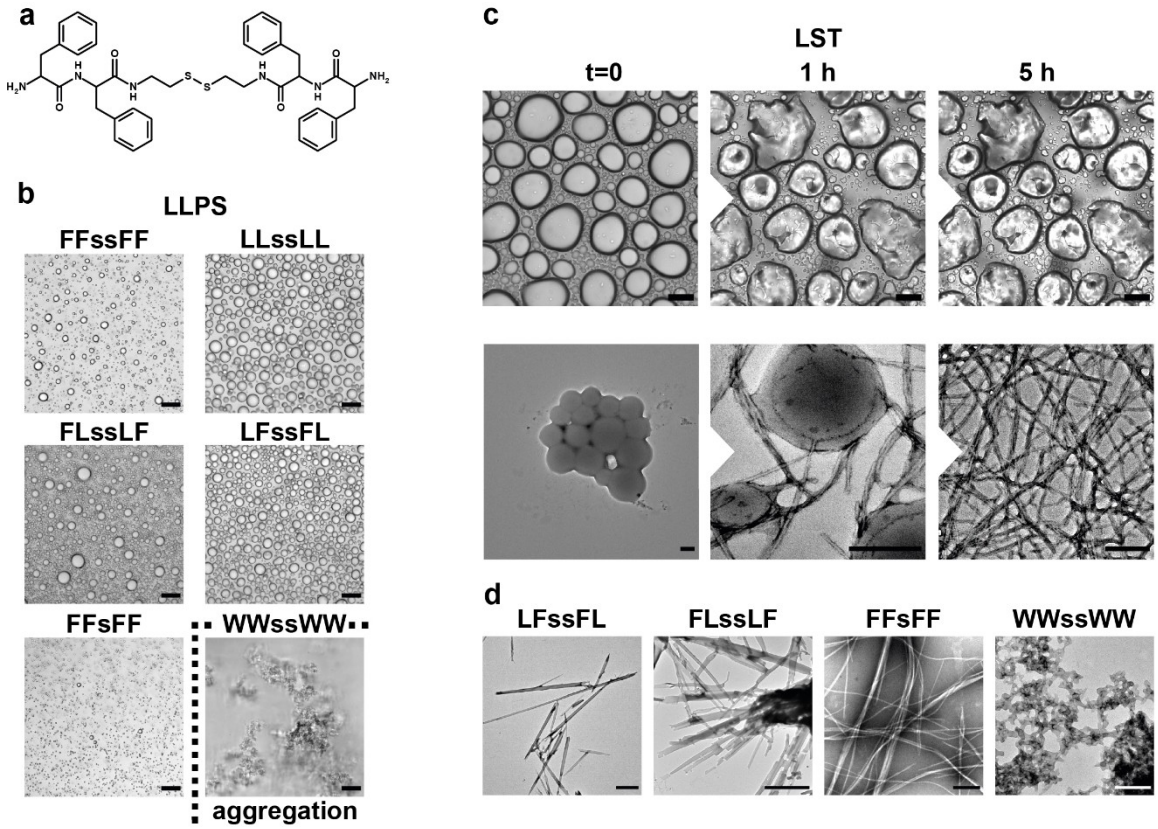

Figure 1. Short peptide derivatives can undergo LST. **(a)** Chemical structure of FFssFF. **(b)** Optical microscope images of samples immediately after inducing phase separation. Only WWssWW forms aggregates immediately, the other derivatives form liquid droplets (scale bar = 20 μm). **(c)** Liquid-to-solid transition of FFssFF condensates followed over time under an optical microscope (upper row, 10 mg/ml FFssFF concentration, scale bar = 20 μm) and under TEM (lower row, 1 mg/ml concentration, scale bar = 200 nm). **(d)** TEM images of aggregates of LFssFL, FLssLF, FFsFF and WWssWW after incubation for 24 h at 37 °C (scale bar = 2 μm for LFssFL and FLssLF, 200 nm for FFsFF and WWsWW).

condensates formed by derivatives with relatively weak stickers (LLssLL) did not change even after 36 h of incubation, suggesting that these derivatives do not undergo LST (Figure S3).

Structural information of the solid aggregates is accessible by solid-state NMR

To obtain more insight into the physical state and molecular structure of these different condensates, we focused on matured condensates of four small peptide derivatives that show distinct phase behaviour. After 24 h of incubation at 37 °C, FFssFF and FFsFF could undergo LLPS followed by a LST yielding ordered fibrils, whereas WWssWW precipitated immediately into amorphous solid aggregates, and LLssLL could also undergo LLPS, but lacked a LST. We studied matured samples of all four derivatives by solid-state NMR.

Figure 2a shows the ^{13}C,^{1}H cross-polarization (CP) spectra measured at 278 K of the compounds without any isotope labelling. In such CP spectra only the immobilized (slow tumbling) species is detected. Broad ^{13}C resonances are detected for WWssWW, but much narrower resonances for FFsFF and particularly for FFssFF. Interestingly, also LLssLL gives signal in CP, with rather sharp resonances for the side-chains and broad resonances for the rest. We attribute the different ^{13}C linewidths to the tendency of the corresponding peptide derivatives to form well-ordered fibril structures as judged from TEM images of the samples (Figure 2b), which show well-defined fibrils for FFssFF and FFsFF in agreement with the narrowest ^{13}C resonances observed, unstructured aggregates for WWssWW and spherical deposits from liquid droplets for LLssLL (for the determined linewidths see Figure S4 and Table S1). Although LLssLL only showed liquid-like coacervates by optical microscopy, a weak CP signal was measured pointing to some fraction of less mobile peptide in these coacervates, eventually pointing to a gel-type phase of liquid droplets induced by the rather high peptide concentration in the NMR rotor (~400 mg/ml). The high resolution and the good signal-to-noise ratio of the ^{13}C spectrum of FFssFF motivated us to continue with more detailed examination of the fibrils formed by this derivative.

FFssFF forms homogeneous fibrils through LST

TEM images of FFssFF aggregates formed by incubation at basic pH reveal the formation of fibrils with a width of around 32 nm

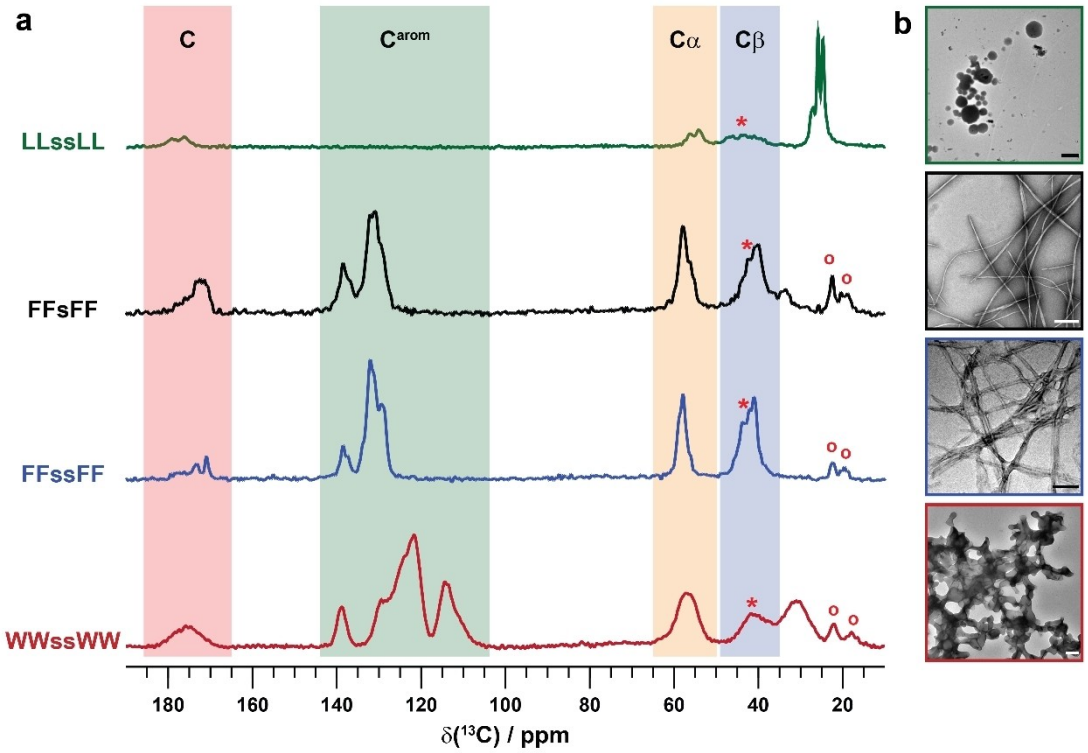

Figure 2. Immobilized species are detected in ^{13}C CP-MAS NMR spectra. **(a)** ^{13}C,^{1}H CP-MAS spectra of matured natural abundance WWssWW (red), FFssFF (blue), FFsFF (black) and LLssLL (green) condensates. All spectra were recorded at 11.7 T and 17 kHz MAS. Red circles indicate sodium-3-(trimethylsilyl)-propanesulfonate (DSS) resonances added for referencing, which slightly vary between the different samples. Red asterisks mark the ^{13}C resonances of the disulphide (for LLssLL, FFssFF and WWssWW) or the thioether linker (for FFsFF). **(b)** TEM images of the samples (scale bar = 2 μm for LLssLL, 200 nm for FFsFF, FFssFF and WWssWW).

(Figure 3a and Figure S5a). The same sample was also analysed using AFM and the average height of the fibrils was determined to be 6.4 nm (Figure 3b and Figure S5b). The difference between the height and the width of the fibrils suggests that each fibril contains several protofilaments (layers of FFssFF molecules stacked together), and resembles a ribbon (which is confirmed by their appearance under TEM, Figure 3a and Figure S5a). The X-ray diffraction (XRD) pattern of a freeze-dried fibril sample (Figure 3c) points to the formation of a structure with cross-β like arrangement, since the pattern resembles that of other amyloid fibrils.[43] The reflexes at 4.8 Å are characteristic of the spacing between two β-strands across the β-sheets along the fibril axis and 11.7 Å is indicative for the spacing perpendicular to the fibril axis.[44]

For a more detailed, atomic-level structural model of the fibrils formed by LST, we investigated the samples further by various solid-state NMR techniques. Our goal was to derive a model of the FFssFF fibrils using distance restraints extracted from solid-state NMR spectra in a structure calculation. We used $^{13}C/^{15}N$ labelled samples in which the phenylalanine residues were isotopically labelled, but the cystamine linker was not. Figure 4a shows the 2D MAS ^{13}C-^{13}C 20 ms dipolar assisted rotational resonance (DARR) spectrum[45,46] in which typically intra-residue correlations are detected. The spectrum reveals four phenylalanine Cα/Cβ correlation peaks in an approximate 1 : 1 : 1 : 1 intensity ratio (see Figure S6) and the observed spectral resolution points to a rather homogeneous sample (which is supported by ^{13}C linewidths, expressed as full width at half maximum, of ≤ 1 ppm). We note that the mentioned intensity ratio was preserved in different samples, thus ruling out the effect of polymorphism on the intensity ratio of such resonances (Figure S6). Negligible polymorphism is however observed and reflected in three sets of resonances with the major polymorph strongly dominating (occurrence of more than 90 %).

Two FF pairs can be sequentially assigned

As a first step towards a structure determination, the backbone resonances were assigned using 2D DARR, NCA and NCO spectra (Figure 4a, b and c and Figure S7a), the phenylalanaine sidechains were assigned by 2D dipolar recoupling enhanced by amplitude modulation (DREAM)[47] and 3D NCACX spectra (Figure S7b, for the chemical shifts see Table S2). A near complete assignment for two FF pairs was achieved (Figure 4e). Note that the linker fragment is not ^{13}C labelled and leads to rather large distances between F2 and F3 (ca. 4 Å between Cα atoms of F1 and F2 vs. ca. 14 Å between Cα atoms of F2 and F3 assuming a linear FFssFF structure) rendering polarization transfer between F2 and F3 impossible (see below). At this stage, we can only speculate that (i) the four resonances can be

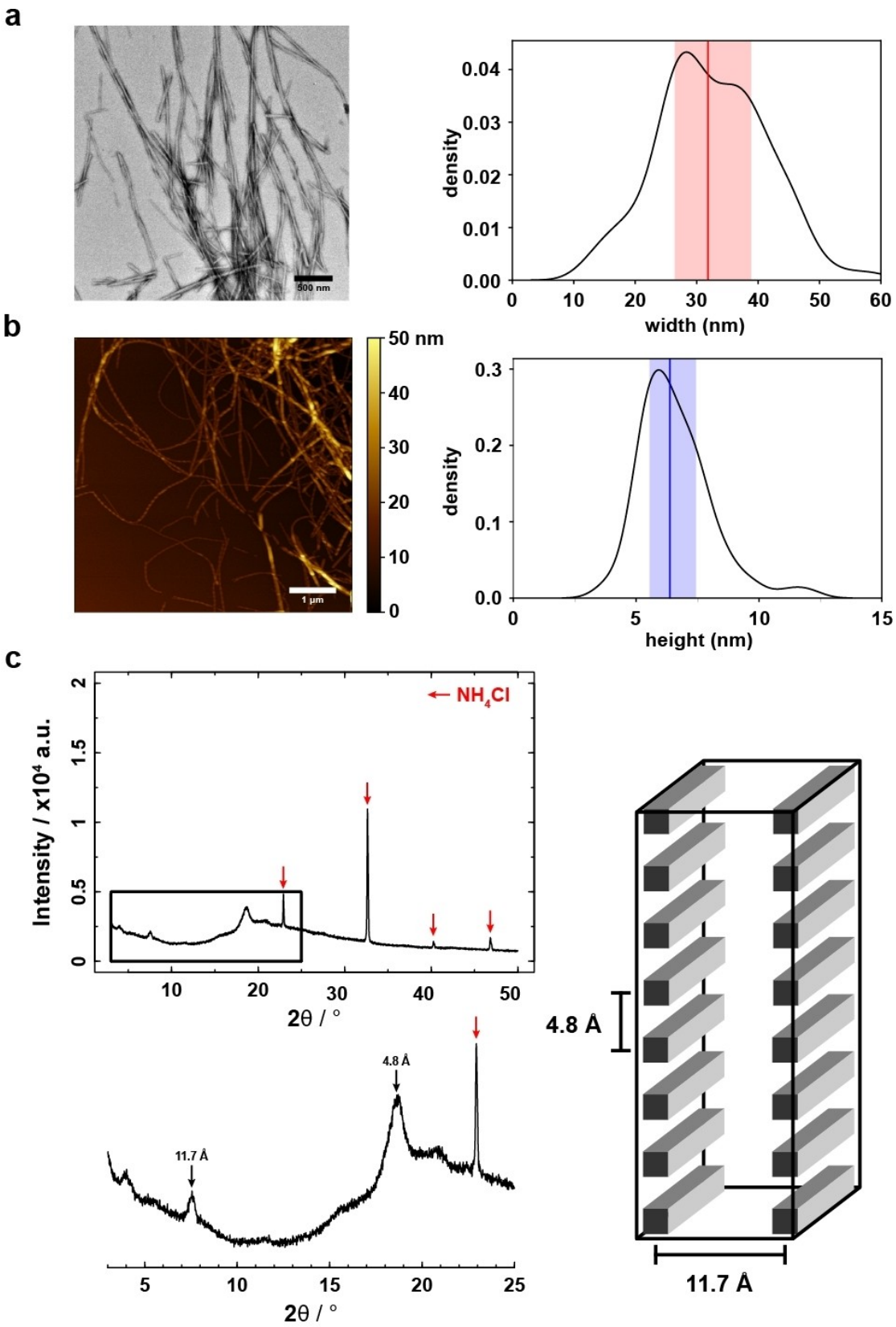

Figure 3. Matured FFssFF condensates form fibrils. **(a)** Representative TEM image of FFssFF fibrils and distribution (kernel density plot, $n = 192$) of fibril width measured from 4 TEM images. The red line indicates the median (32 nm) and the shaded area corresponds to the range between the 1st and 3rd quartile. **(b)** AFM height image of FFssFF fibrils and distribution (kernel density plot, $n = 75$) of fibril height measured from the AFM image. The blue line indicates the median (6.4 nm) and the shaded area corresponds to the range between 1st and 3rd quartile. **(c)** X-ray diffraction pattern revealing distances of 4.8 Å and 11.7 Å as expected for a fibrillar arrangement as shown schematically on the right. The red arrows indicate NH_4Cl reflexes.

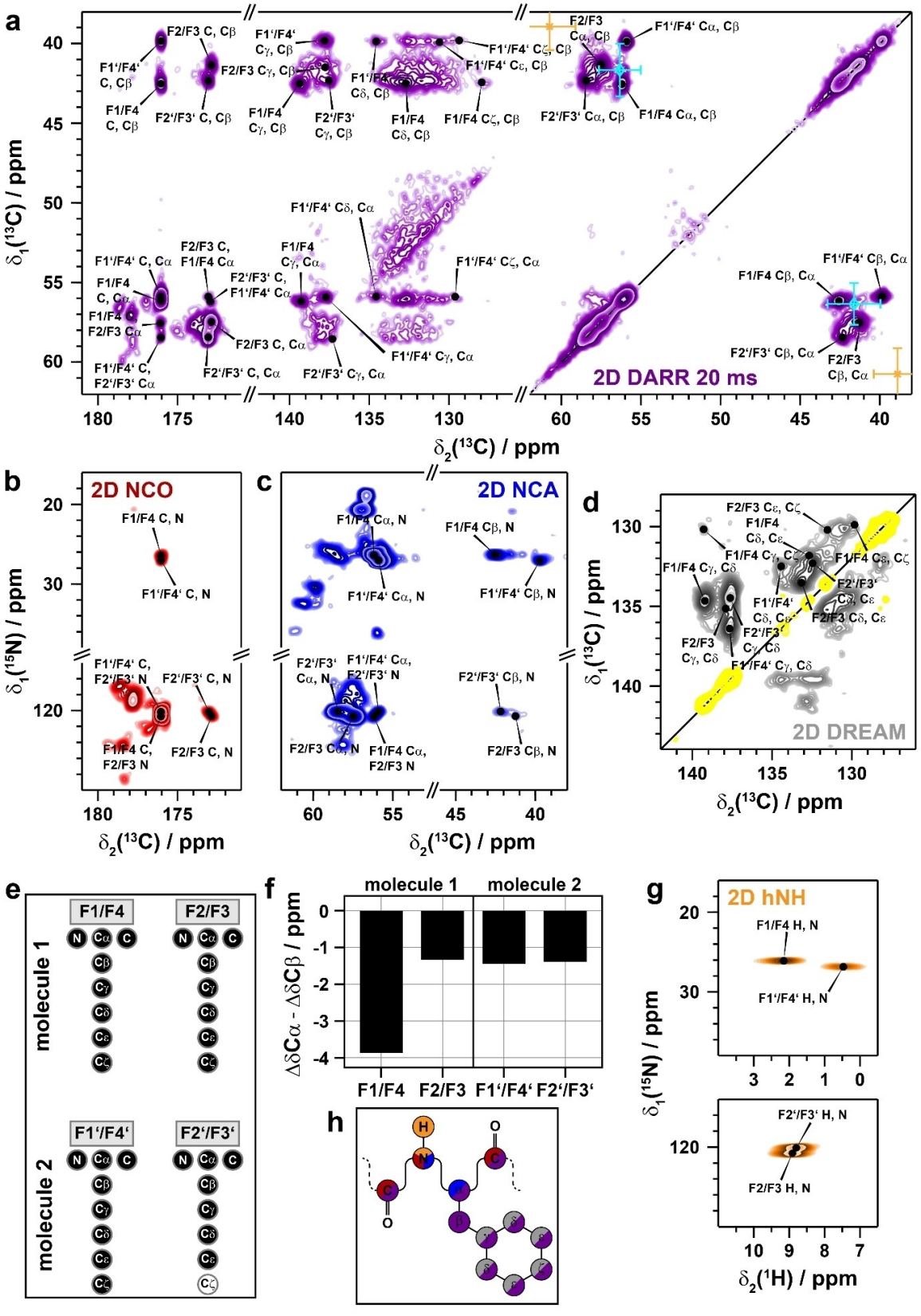

Figure 4. Fibrillized FFssFF yields resolved solid-state NMR spectra indicating the formation of homogeneous fibrils. **(a)** 2D ^{13}C-^{13}C 20 ms DARR (orange and cyan dots with error bars indicate the average Cα/Cβ chemical-shift values for Phe in α-helixes and β-sheets, respectively),[56] **(b)** ^{15}N-^{13}C NCO, **(c)** ^{15}N-^{13}C NCA, **(d)** ^{13}C-^{13}C DREAM spectrum showing the aromatic region (negative contour levels are plotted in grey, positive contour levels in yellow). **(e)** Resonance assignment graph. **(f)** Secondary chemical-shift analysis (chemical shifts of the random coil conformation are taken from Ref. [56]). **(g)** ^{15}N,^{1}H hNH spectrum. **(h)** Schematic representation of phenylalanine resonances and their appearance in the solid-state NMR spectra using the color-coding used for the individual spectra.

assigned to a FFssFF molecule in which the structural symmetry between the two halves is broken, for example by intermolecular packing interactions,[48–50] or, (ii) that they can be assigned to two FFssFF molecules (each of them possessing a local C_2 symmetry) that are structurally distinct.[51–53] The latter hypothesis seems reasonable in light of the several layers of FFssFF molecules that are present as judged from the TEM data, and that structurally distinct molecules with corresponding peak splitting in NMR spectra have also been reported in the context of amyloid fibrils.[52,53] In the following sections we therefore chose to label the residues of the (C_2-symmetric) molecules 1 and 2 by F1/F4 and F2/F3 or F1′/F4′ and F2′/F3′, respectively (Figure 4). However, we note that a definite answer remains elusive by our solid-state NMR studies.

Backbone secondary chemical shifts point to β-strand-like backbone conformation

The conformation of the peptide backbone can be assessed by solid-state NMR due to the dependence of the Cα/Cβ chemical-shift values on dihedral angles.[54,55] Figure 4f shows the secondary chemical-shift analysis for FFssFF fibrils. Although, strictly speaking, more than three residues downstream of a reference residue with negative secondary chemical shifts are required to identify a sequence as β-strand,[55] we conclude that the negative secondary chemical-shift values observed here for all phenylalanine residues points to a backbone conformation in the FFssFF molecules that is "β-strand-like", in good agreement with the XRD analysis (Figure 3c). This is further supported by plotting the statistical distribution of averaged Phe ^{13}C Cα/Cβ chemical-shift values for the different secondary structure elements on the spectrum (Figure 4a).[56] Based on the secondary chemical-shift analysis, we assume typical dihedral angles of β-strand for F2/F3 and F2′/F3′ ($\varphi = 140°$ and $\psi = -125°$) in the structure calculations (see below). Interestingly, the results for the terminal phenylalanine residues (either in the same or in two different molecules) are quite different (secondary chemical shifts of −4 ppm compared to −1.5 ppm). A similar observation is made in ^{1}H-detected hNH spectra using an MAS frequency of 40 kHz (Figure 4g). The primary amine ($-NH_2$) proton chemical-shift values of F1/F4 and F1′/F4′ differ by around 2 ppm whose origin remains currently unclear (see also Table S3).

Long-range distance restraints for structural modelling

We next determined long-range distance restraints required for the structure calculation. Such restraints were obtained from a uniformly labelled sample (using 150 ms DARR and 400 μs spin-diffusion based CHHC experiments[57]) and a ^{13}C:^{15}N 1:1 mixed labelled sample (using NCA, NCO, 6 ms proton-assisted insensitive nuclei cross-polarization (PAIN),[58] 500 μs NHHC,[57] 150 ms DARR and 400 μs CHHC experiments, see Figure S8). Unfortunately, a diluted sample (^{13}C labelled peptide diluted in ^{15}N labelled peptide with a ratio of 1:2.5) required for unambigously distinguishing intra- and intermolecular correlations observed in uniformly labelled samples yielded another polymorph in several efforts (see Figure S9).

Of particular importance are the 2D NCA and NCO spectra performed on the mixed labelled sample, which probe ^{13}C,^{15}N intermolecular contacts (Figure S8e and f). We observe strong intermolecular correlations in the 2D NCA spectrum between backbone nitrogen and Cα atoms of the same residue ($i \rightarrow i$) pointing to rather short intermolecular contacts and already suggesting a top-on-top alignment of the molecules, which in amyloid fibrils is often denoted as "in-register" parallel stacking. This is further supported by intermolecular $i \rightarrow i+1$ backbone nitrogen and CO correlations observed in the NCO spectrum (Figure S8f). We also recorded a ^{13}C,^{15}N PAIN[58] spectrum on the mixed labelled sample, which is typically used in amyloid fibrils to probe intermolecular interactions along the fibril axis[59] (Figure 5a, pale red spectrum) and compared it with the NCA spectrum of the uniformly labelled sample (Figure 5a, blue spectrum), in which intense intraresidual correlations are detected. If the peak positions of the NCA and PAIN spectra match, the residues are stacked directly on top of each other, which is indeed observed in the present case (Figure 5a and Figure 5b). Note that in the PAIN spectrum also intermolecular $i \rightarrow i+1$ contacts are observed. Finally, it is important to mention that in all spectra no intermolecular long-range correlations between the two sets of resonances can be observed (e.g. no contacts between F1/F4 and F1′/F4′).

Phenylalanine sidechain π-π interactions are involved in phase separation and fibril formation

As a consecutive step, we performed a structure calculation with CYANA, a software package used for structural modelling of proteins based on distance restraints derived from multi-dimensional solution-state, as well as solid-state NMR spectra.[60,61] Herein, six FFssFF molecules and the determined distance restraints for the two C_2-symmetric molecules 1 and 2 (108 and 112 in total, for a graphical representation of these restraints on the structural model, see Figure S10 and Figure S11, for the distance restraints and further parameters of the calculation see Tables S4 and S5) were employed. For the calculation, we assume scenario (ii), a C_2 symmetry within the molecule, which we implemented in the calculation by mirroring the distance restraints for the two halves of the molecule. All distance restraints can be fulfilled, which leads to small values of the CYANA target function (0.06 and 0.59 Å^2 for ladders formed of molecule 1 and 2, respectively).

The resulting structural models for the two FFssFF ladders are shown in Figure 5c and clearly show a parallel alignment of molecules along the fibril axis. Interestingly, in the energetically most favoured state, the arrangement of the phenylalanine rings suggests π-π stacking interactions between them (note that no intermolecular restraints between the aromatic rings were explicitly used in the calculations). It is reasonable to assume that these noncovalent interactions stabilize the fibrilar aggregates of FFssFF, in agreement with our previous findings that LLssLL does not display a LST under studied conditions. It

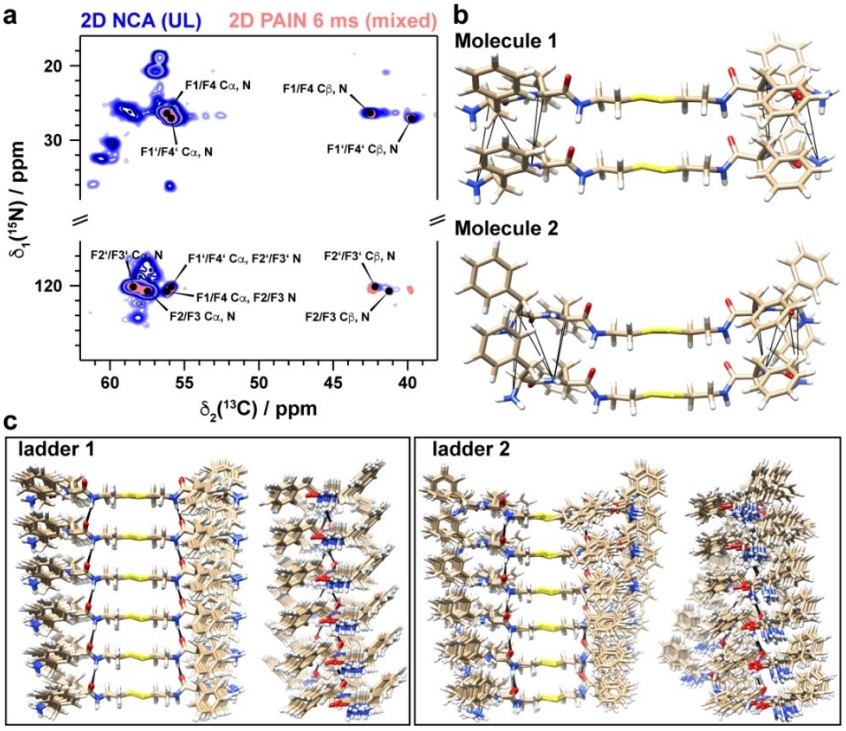

Figure 5. Structural model of FFssFF fibrils from solid-state NMR distance restraints. **(a)** Superposition of the NCA spectrum of UL ^{13}C,^{15}N-labeled fibrils (blue) and the PAIN spectrum of mixed ^{13}C- and ^{15}N-labeled fibrils (pale red). The superposition of cross peaks indicates a parallel alignment of the molecules along the fibril axis. **(b)** Parallel alignment of FFssFF molecules with the distance restraints determined from the PAIN spectrum for both molecules. **(c)** Lowest energy structure bundles, shown in two different orientations, for ladders **1** and **2** obtained by CYANA calculations.

is plausible that a lower degree of π-π stacking interactions initially drives LLPS, which can subsequently be rearranged in the dense liquid droplets leading to nucleation and growth of ordered fibrils. The fact that under studied conditions LLPS can precede fibril formation in these and other systems is likely due to the fact that some of the aromatic groups are more spatially restricted than others, and have a higher energy barrier. The liquid condensed state represents a highly concentrated environment in which nucleation of amyloid-like fibrils is more likely.[11,12,62–64] These results pinpoint to the important role of π-π interactions and steric effects in both LLPS and LST.[19,34] It is reasonable to assume that the two FFssFF ladders belong to different protofilaments[65,66] both being part of the same fibril and are thus not caused by polymorphism (see above). Our solid-state NMR spectra, however, do not reveal any inter-protofilament contacts. Probing such contacts by classical dipolar coupling-based solid-state NMR techniques is highly challenging[67] and in this particular case even more complicated due to overlapping resonances in the purely phenylalanine-containing construct.

Conclusions

By means of NMR, microscopy and XRD we investigated the structures of solid and liquid condensates formed by several short peptide derivatives. Derivatives precipitating immediately into solid aggregates exhibit a disordered amorphous structure, while derivatives undergoing LLPS form liquid-like droplets that can further transform into solid, fibrillar aggregates with well-defined, amyloid-like structure. TEM images show that fibrils emerge from condensed droplets, suggesting that they are nucleated inside the droplets or at their interface. The fibrils are relatively thick (ca. 32 nm in diameter), pointing to several protofilaments within the fibril, in agreement with previous reports for fibrillar structures of similar short peptides.[68,69] NMR and XRD experiments showed that the molecules are oriented top-on-top ("in-register") along the fibril axis. Polymorphism, a common phenomenon in amyloid fibril formation,[55] has been observed as well, but we found that one polymorph was always strongly dominating, pointing to a highly directive LST process. Interestingly, NMR experiments suggest the presence of four chemically distinct phenylalanine residues, appearing always with fixed intensity ratio of 1 : 1 : 1 : 1. This can be explained by (i) self-assembly of FFssFF into fibrils resulting in breaking of the molecular C_2-symmetry; or (ii) self-assembly into two FFssFF ladders, in which the molecular C_2-symmetry is preserved for the two molecules, but which are chemically distinct from each other due to their arrangement within the fibril. Structural modelling of FFssFF based on the collected solid-state NMR distance restraints confirms the top-to-top alignment of molecules along the fibril axis, with peptide backbone angles resembling that of β-sheets in larger peptides. In the energetically most favoured state, a geometry favouring π-π stacking of the phenylalanine rings is observed in both calculated models for the two FFssFF ladders detected, which suggests that these

interactions stabilise the fibril structure and might be the driving force for the LST process and probably also promote LLPS.[19,20,70–73] As we observed that substitution of phenylalanine residues for leucine residues hampers LST, we hypothesise that while π-π interactions are crucial for fibril formation, hydrophobic interactions are enough to already promote LLPS. Since the design of the studied molecules is based on the simplified sticker-spacer model typical for proteins undergoing LLPS and the structure of fibrils resembles amyloids, our results may suggest that similar stabilisation through π-π interactions may be also responsible for the LST of membraneless organelles in cells.

Experimental Section

Reagents: Unless specified otherwise, reagents were obtained from Sigma Aldrich. All peptide derivatives studied here (FFssFF, FFsFF, LLssLL and WWssWW) were synthesised in solution using L-amino acids and Boc/HATU chemistry as described before.[35] Isotopically labelled variants of FFssFF were synthesized according to the same protocol, using ^{15}N, ^{13}C and double $^{13}C/^{15}N$ labelled Boc–L-Phe–OH. Isotopically labelled Boc–L-Phe–OH was obtained from L-phenylalanine with a minimal isotopic purity of 98% purchased from Sigma Aldrich, using di-tert-butyl dicarbonate, according to the protocol described elsewhere.[66] For the 1:1 mixed-labelled sample, ^{13}C-labelled FFssFF was mixed with ^{15}N-labelled FFssFF in a 1:1 molar ratio. For the ^{13}C-diluted sample, ^{13}C-labelled FFssFF was mixed with ^{15}N-labelled FFssFF in a 1:2.5 molar ratio.

Sample preparation: Samples for the NMR studies were prepared by dissolving peptide derivatives at a concentration of 10 mg/ml (experiment with derivatives containing different amino acids) or at 6 mg/ml (experiments with different labelled FFssFF samples), filtering the solution (cellulose acetate filter, 0.45 μm pore size), precipitating by adding 0.4 M or 1 M NaOH to the final concentration of 16 or 12 mM (respectively for 10 mg/ml and 6 mg/ml solutions) and subsequent incubation in a thermoshaker for 24 h (37 °C, orbital shaking at 600 rpm). Samples for TEM and AFM were prepared by dissolving peptide derivatives at a concentration of 1 mg/ml, filtering the solution (cellulose acetate filter, 0.45 μm pore size), precipitating by adding 1 M NaOH to the final concentration of 2 mM and subsequent incubation in a thermoshaker for 24 h (37 °C, orbital shaking at 600 rpm). Samples for optical microscopy were prepared by dissolving peptide derivatives at a concentration of 10 mg/ml, filtering the solution (cellulose acetate filter, 0.45 μm pore size), precipitating by adding 1 M NaOH to the final concentration of 16 mM and subsequent incubation in a thermoshaker for 24 h (37 °C, orbital shaking at 600 rpm). Samples for X-ray diffraction were prepared by dissolving peptide derivatives at a concentration of 6 mg/ml, filtering the solution (cellulose acetate filter, 0.45 μm pore size), precipitating by adding 1 M ammonium hydroxide to the final concentration of 12 mM, subsequent incubation in a thermoshaker for 24 h (37 °C, orbital shaking at 600 rpm) and freeze drying the obtained aggregate.

NMR sample preparation: All peptide derivative solutions were sedimented[74–77] in the MAS NMR rotor (16 h at 4 °C at 210,000×*g*) using home-built tools.[78] A summary of the samples is given in Table 1.

Solid-state NMR: ^{1}H- and ^{13}C-detected solid-state NMR spectra were acquired at 11.7 and 20.0 T static magnetic field strength using 1.9 and 3.2 mm Bruker Biospin probes. The MAS frequency was set to 17 and 40 kHz. The sample temperature was set to ~5 and 30 °C using the water line as an internal reference for the measurements in 3.2 and 1.9 mm rotors, respectively.[78] The spectra were processed with the software TOPSPIN (version 3.5, Bruker Biospin) with a shifted (2.5 to 5.0) squared cosine apodization function and automated baseline correction in the indirect and direct dimensions. An overview of the experimental parameters for all NMR spectra is given in Table S4. Spectra were analysed with the software CcpNmr (version: 2.4.2)[79–81] and referenced to sodium-3-(trimethylsilyl)propanesulfonate (DSS).

Table 1. Summary of the prepared solid-state NMR samples. NA: natural abundance. UL: uniformly labeled.

sample	isotope labeling scheme	rotor diameter/mm
LLssLL	NA	3.2
FFsFF	NA	3.2
FFssFF	NA	3.2
WWssWW	NA	3.2
FFssFF	UL	1.9
FFssFF	Mixed (^{13}C:^{15}N = 1:1)	1.9
FFssFF	Diluted (^{13}C:^{15}N = 1:2.5)	1.9

CYANA calculations: All structure calculations were performed with CYANA (version 3.98.13).[60,61] The residue library was expanded by the molecule construct for FFss. This molecule has been created with the program Avogadro (version 1.2).[82] For each CYANA calculation, two molecule constructs of FFss are needed to generate a full FFssFF molecule. The two constructs are connected with each other by overlaying corresponding atoms in the S–S linker. A C_2-symmetry is used to generate a highly symmetric molecule along the fibril axis. The used distance restraints with their upper distance limits[25,27] are summarized in Tables S5 and S6. The CYANA code and the residue library of FFss are given in the Supporting Information, Table S7.

X-ray diffraction: The diffractograms were measured on a Panalytical Empyrean diffractometer in Debye–Scherrer transmission geometry (capillary mode) using monochromatic Cu Kα radiation (1.541 Å) from a sealed LFF tube (operating voltage of 45 kV, current 40 mA), a focusing X-ray mirror (elliptic, W/Si) and a PIXcel3D 1x1 detector. A continuous scan was made in the $2° < 2\theta < 35°$ range with a step size of 0.013°. A freeze-dried sample of FFssFF fibrils was placed in a 0.5 mm soda lime glass capillary and sealed hermetically using super glue.

TEM measurements: Post incubation, suspension of phase-separated sample (5 μL) was transferred onto a TEM grid (EM-Tec carbon support film on copper, 300 square mesh, Micro to Nano, the Netherlands). Samples were blotted with filter paper, stained with 5 μL of 2% (w/w) sodium phosphotungstate solution (adjusted to pH 7.4), washed with 5 μL of water and left to dry overnight. Imagining was performed using JEOL JEM-1400 FLASH. For the time-resolved liquid-to-solid transition experiment, samples were collected at specified time points during incubation.

AFM measurements: Post incubation, suspension of phase-separated sample (10 μL) was transferred onto a mica disc (Nano-Tec V-1 grade muscovite mica discs, Micro to Nano, the Netherlands), blotted with filter paper, washed with 10 μL of milliQ water and left to dry overnight. AFM images were collected in tapping mode on a Veeco Dimension 3000 AFM, using SSS-NCHR-SPL silicon tips (Nanosensors, Switzerland). Images were analyzed in Gwyddion 2.56.

Supporting Information

Additional references cited within the Supporting Information.[83,84]

Author Contributions

W.L. synthesized all compounds, prepared the samples and performed TEM and AFM measurements. J.Z. performed the NMR experiments and carried out the CYANA calculations together with P.G. M.A. contributed to the original synthesis and microscopy investigation. All authors have analysed data and have contributed to the writing of the article. E.S. and T.W. designed and supervised the study.

Acknowledgements

T.W. acknowledges support from an ETH research grant (ETH-43 17-2, funding for J.Z.) and the Deutsche Forschungsgemeinschaft (DFG, German Research Foundation, project number 455240421 and Heisenberg fellowship, project number 455238107). T.W. acknowledges the Max Planck Society for funding. E.S. acknowledges financial support from the European Research Council (ERC) under the European Union's Horizon 2020 research and innovation programme (grant agreement number 851963). We thank Paul Tinnemans (Radboud University) for performing X-ray diffraction measurements and for help with their interpretation. We also thank Geert-Jan Janssen (Radboud University) for help with TEM measurements, Marc Stuart (University of Groningen) for help with the interpretation of the TEM data, and Ettore Bartalucci (MPI CEC, Mülheim) for discussions and providing a script to analyze secondary chemical-shift values. We also thank Dr. Wörle (ETH Zürich, Switzerland) for measuring additional X-ray diffraction data (not shown in the manuscript). Open Access funding enabled and organized by Projekt DEAL.

Conflict of Interests

The authors declare no conflict of interest.

Data Availability Statement

The data that support the findings of this study are available from the corresponding author upon reasonable request.

Keywords: droplet · fibril · noncovalent interactions · phase transitions · solid-state NMR

[1] D. M. Mitrea, R. W. Kriwacki, *Cell Commun. Signaling* **2016**, *14*, 1–20.
[2] E. Gomes, J. Shorter, *J. Biol. Chem.* **2019**, *294*, 7115–7127.
[3] C. Greening, T. Lithgow, *Nat. Rev. Microbiol.* **2020**, *18*, 677–689.
[4] C. A. Azaldegui, A. G. Vecchiarelli, J. S. Biteen, *Biophys. J.* **2021**, *120*, 1123–1138.
[5] A. A. Hyman, C. A. Weber, F. Jülicher, *Annu. Rev. Cell Dev. Biol.* **2014**, *30*, 39–58.
[6] E. Boke, M. Ruer, M. Wühr, M. Coughlin, R. Lemaitre, S. P. Gygi, S. Alberti, D. Drechsel, A. A. Hyman, T. J. Mitchison, *Cell* **2016**, *166*, 637–650.
[7] M. Falk, Y. Feodorova, N. Naumova, M. Imakaev, B. R. Lajoie, H. Leonhardt, B. Joffe, J. Dekker, G. Fudenberg, I. Solovei, L. A. Mirny, *Nature* **2019**, *570*, 395–399.
[8] S. Alberti, S. Carra, *J. Mol. Biol.* **2018**, *430*, 4711–4729.
[9] W. M. Babinchak, W. K. Surewicz, *J. Mol. Biol.* **2020**, *432*, 1910–1925.
[10] S. C. Ling, M. Polymenidou, D. W. Cleveland, *Neuron* **2013**, *79*, 416–438.
[11] A. Patel, H. O. Lee, L. Jawerth, S. Maharana, M. Jahnel, M. Y. Hein, S. Stoynov, J. Mahamid, S. Saha, T. M. Franzmann, A. Pozniakovski, I. Poser, N. Maghelli, L. A. Royer, M. Weigert, E. W. Myers, S. Grill, D. Drechsel, A. A. Hyman, S. Alberti, *Cell* **2015**, *162*, 1066–1077.
[12] S. Wegmann, B. Eftekharzadeh, K. Tepper, K. M. Zoltowska, R. E. Bennett, S. Dujardin, P. R. Laskowski, D. MacKenzie, T. Kamath, C. Commins, C. Vanderburg, A. D. Roe, Z. Fan, A. M. Molliex, A. Hernandez-Vega, D. Muller, A. A. Hyman, E. Mandelkow, J. P. Taylor, B. T. Hyman, *EMBO J.* **2018**, *37*, e98049.
[13] A. Molliex, J. Temirov, J. Lee, M. Coughlin, A. P. Kanagaraj, H. J. Kim, T. Mittag, J. P. Taylor, *Cell* **2015**, *163*, 123–133.
[14] P. Li, S. Banjade, H.-C. C. Cheng, S. Kim, B. Chen, L. Guo, M. Llaguno, J. V. Hollingsworth, D. S. King, S. F. Banani, P. S. Russo, Q.-X. X. Jiang, B. T. Nixon, M. K. Rosen, *Nature* **2012**, *483*, 336–340.
[15] M. Kato, T. W. Han, S. Xie, K. Shi, X. Du, L. C. Wu, H. Mirzaei, E. J. Goldsmith, J. Longgood, J. Pei, N. V. Grishin, D. E. Frantz, J. W. Schneider, S. Chen, L. Li, M. R. Sawaya, D. Eisenberg, R. Tycko, S. L. McKnight, *Cell* **2012**, *149*, 753–767.
[16] H. Zhang, S. Elbaum-Garfinkle, E. M. Langdon, N. Taylor, P. Occhipinti, A. A. Bridges, C. P. Brangwynne, A. S. Gladfelter, *Mol. Cell* **2015**, *60*, 220–230.
[17] Y. Shin, C. P. Brangwynne, *Science* **2017**, *357*, eaaf4382.
[18] S. F. Banani, H. O. Lee, A. A. Hyman, M. K. Rosen, *Nat. Rev. Mol. Cell Biol.* **2017**, *18*, 285–298.
[19] J. Wang, J. M. Choi, A. S. Holehouse, H. O. Lee, X. Zhang, M. Jahnel, S. Maharana, R. Lemaitre, A. Pozniakovsky, D. Drechsel, I. Poser, R. V. Pappu, S. Alberti, A. A. Hyman, *Cell* **2018**, *174*, 688–699.e16.
[20] E. W. Martin, A. S. Holehouse, I. Peran, M. Farag, J. J. Incicco, A. Bremer, C. R. Grace, A. Soranno, R. V. Pappu, T. Mittag, *Science* **2020**, *367*, 694–699.
[21] L. Emmanouilidis, L. Esteban-Hofer, G. Jeschke, F. H.-T. Allain, *Curr. Opin. Struct. Biol.* **2021**, *70*, 132–138.
[22] L. Emmanouilidis, L. Esteban-Hofer, F. F. Damberger, T. de Vries, C. K. X. Nguyen, L. F. Ibáñez, S. Mergenthal, E. Klotzsch, M. Yulikov, G. Jeschke, F. H.-T. Allain, *Nat. Chem. Biol.* **2021**, *17*, 608–614.
[23] Y. Shen, A. Chen, W. Wang, Y. Shen, F. Simone Ruggeri, S. Aime, Z. Wang, S. Qamar, J. R. Espinosa, A. Garaizar, P. St George-Hyslop, R. Collepardo-Guevara, D. A. Weitz, D. Vigolo, T. P. J. Knowles, *Bioarxiv* **2022**, 10.1101/2022.08.15.503964.
[24] S. Ranganathan, E. Shakhnovich, *Biophys. J.* **2022**, *121*, 2751–2766.
[25] M. A. Wälti, F. Ravotti, H. Arai, C. G. Glabe, J. S. Wall, A. Böckmann, P. Güntert, B. H. Meier, R. Riek, *Proc. Natl. Acad. Sci. USA* **2016**, *113*, E4976-E4984.
[26] M. T. Colvin, R. Silvers, Q. Z. Ni, T. V. Can, I. Sergeyev, M. Rosay, K. J. Donovan, B. Michael, J. Wall, S. Linse, R. G. Griffin, *J. Am. Chem. Soc.* **2016**, *138*, 9663–9674.
[27] H. Van Melckebeke, C. Wasmer, A. Lange, E. Ab, A. Loquet, A. Böckmann, B. H. Meier, *J. Am. Chem. Soc.* **2010**, *132*, 13765–13775.
[28] D. T. Murray, M. Kato, Y. Lin, K. R. Thurber, I. Hung, S. L. McKnight, R. Tycko, *Cell* **2017**, *171*, 615–627.e16.
[29] C. Seuring, J. Verasdonck, J. Gath, D. Ghosh, N. Nespovitaya, M. A. Wälti, S. K. Maji, R. Cadalbert, P. Güntert, B. H. Meier, R. Riek, *Nat. Struct. Mol. Biol.* **2020**, *27*, 1178–1184.
[30] A. K. Schütz, T. Vagt, M. Huber, O. Y. Ovchinnikova, R. Cadalbert, J. Wall, P. Güntert, A. Bcöckmann, R. Glockshuber, B. H. Meier, *Angew. Chem. Int. Ed.* **2015**, *54*, 331–335.
[31] R. F. Berkeley, M. Kashefi, G. T. Debelouchina, *Biophys. J.* **2021**, *120*, 1276–1287.
[32] R. Damman, S. Schütz, Y. Luo, M. Weingarth, R. Sprangers, M. Baldus, *Nat. Commun.* **2019**, *10*, 1–11.
[33] S. E. Reichheld, L. D. Muiznieks, F. W. Keeley, S. Sharpe, *Proc. Nat. Acad. Sci.* **2017**, *114*, E4408–E4415.

[34] B. Gabryelczyk, H. Cai, X. Shi, Y. Sun, P. J. M. Swinkels, S. Salentinig, K. Pervushin, A. Miserez, *Nat. Commun.* **2019**, *10*, 1–12.
[35] E. Gibbs, B. Perrone, A. Hassan, R. Kümmerle, R. Kriwacki, *J. Magn. Reson.* **2020**, *310*, 106646.
[36] A. C. Murthy, N. L. Fawzi, *J. Biol. Chem.* **2020**, *295*, 2375–2384.
[37] Y. Wittmer, K. M. Jami, R. K. Stowell, T. Le, I. Hung, D. T. Murray, *J. Am. Chem. Soc.* **2023**, *145*, 1580–1592.
[38] J. Gath, L. Bousset, B. Habenstein, R. Melki, A. Böckmann, B. H. Meier, *PLoS One* **2014**, *9*, e90659.
[39] C. Wasmer, A. Soragni, R. Sabaté, A. Lange, R. Riek, B. H. Meier, *Angew. Chem. Int. Ed.* **2008**, *47*, 5839–5841.
[40] M. Abbas, W. P. Lipiński, K. K. Nakashima, W. T. S. Huck, E. Spruijt, *Nat. Chem.* **2021**, *13*, 1046–1054.
[41] Y. Shen, F. S. Ruggeri, D. Vigolo, A. Kamada, S. Qamar, A. Levin, C. Iserman, S. Alberti, P. S. George-Hyslop, T. P. J. Knowles, *Nat. Nanotechnol.* **2020**, *15*, 841–847.
[42] M. Linsenmeier, L. Faltova, U. C. Palmiero, C. Seiffert, A. M. Küffner, D. Pinotsi, J. Zhou, R. Mezzenga, P. Arosio, *bioRxiv* **2022**, 2022.05.23.493075.
[43] M. Sunde, L. C. Serpell, M. Bartlam, P. E. Fraser, M. B. Pepys, C. C. F. Blake, *J. Mol. Biol.* **1997**, *273*, 729–739.
[44] A. W. P. Fitzpatrick, G. T. Debelouchina, M. J. Bayro, D. K. Clare, M. A. Caporini, V. S. Bajaj, C. P. Jaroniec, L. Wang, V. Ladizhansky, S. A. Müller, C. E. MacPhee, C. A. Waudby, H. R. Mott, A. De Simone, T. P. J. Knowles, H. R. Saibil, M. Vendruscolo, E. V. Orlova, R. G. Griffin, C. M. Dobson, *Proc. Natl. Acad. Sci. USA* **2013**, *110*, 5468–5473.
[45] K. Takegoshi, S. Nakamura, T. Terao, *Chem. Phys. Lett.* **1999**, *307*, 295–302.
[46] K. Takegoshi, S. Nakamura, T. Terao, *Chem. Phys. Lett.* **2001**, *344*, 631–637.
[47] R. Verel, M. Ernst, B. H. Meier, *J. Magn. Reson.* **2001**, *150*, 81–99.
[48] K. Ziach, J. Jurczak, *Chem. Commun.* **2015**, *51*, 4306–4309.
[49] T. Matsuura, H. Koshima, *J. Photochem. Photobiol. C* **2005**, *6*, 7–24.
[50] V. Sagar, G. Wistow, *J. Mol. Biol.* **2022**, *434*, 167559.
[51] J. T. Nielsen, M. Bjerring, M. D. Jeppesen, R. O. Pedersen, J. M. Pedersen, K. L. Hein, T. Vosegaard, T. Skrydstrup, D. E. Otzen, N. C. Nielsen, *Angew. Chem.* **2009**, *121*, 2152–2155.
[52] C. Sachse, M. Fändrich, N. Grigorieff, *Proc. Natl. Acad. Sci. USA* **2008**, *105*, 7462–7466.
[53] J. M. Lopez Del Amo, M. Schmidt, U. Fink, M. Dasari, M. Fändrich, B. Reif, *Angew. Chem. Int. Ed.* **2012**, *51*, 6136–6139.
[54] S. Spera, A. Bax, *J. Am. Chem. Soc.* **1991**, *113*, 5490–5492.
[55] Y. Shen, F. Delaglio, G. Cornilescu, A. Bax, *J. Biomol. NMR* **2009**, *44*, 213–223.
[56] Y. Wang, O. Jardetzky, *Protein Sci.* **2002**, *11*, 852.
[57] A. Lange, S. Luca, M. Baldus, *J. Am. Chem. Soc.* **2002**, *124*, 9704–9705.
[58] J. R. Lewandowski, G. De Paëpe, R. G. Griffin, *J. Am. Chem. Soc.* **2007**, *129*, 728–729.
[59] L. Lecoq, T. Wiegand, F. J. Rodriguez-Alvarez, R. Cadalbert, G. A. Herrera, L. del Pozo-Yauner, B. H. Meier, A. Böckmann, *ChemBioChem* **2019**, *20*, 1027–1031.
[60] P. Güntert, C. Mumenthaler, K. Wüthrich, *J. Mol. Biol.* **1997**, *273*, 283–298.
[61] P. Güntert, L. Buchner, *J. Biomol. NMR* **2015**, *62*, 453–471.
[62] W. M. Babinchak, R. Haider, B. K. Dumm, P. Sarkar, K. Surewicz, J.-K. K. Choi, W. K. Surewicz, *J. Biol. Chem.* **2019**, *294*, 6306–6317.
[63] S. Ray, N. Singh, R. Kumar, K. Patel, S. Pandey, D. Datta, J. Mahato, R. Panigrahi, A. Navalkar, S. Mehra, L. Gadhe, D. Chatterjee, A. S. Sawner, S. Maiti, S. Bhatia, J. A. Gerez, A. Chowdhury, A. Kumar, R. Padinhateeri, R. Riek, G. Krishnamoorthy, S. K. Maji, *Nat. Chem.* **2020**, *12*, 705–716.
[64] S. Ray, D. Chatterjee, S. Mukherjee, K. Patel, J. Mahato, S. Kadam, R. Krishnan, A. S. Sawner, M. Poudyal, G. Krishnamoorthy, A. Chowdhury, R. Padinhateeri, S. K. Maji, *BioRxiv* **2021**, *4*, 6.
[65] L. C. Serpell, M. Sunde, M. D. Benson, G. A. Tennent, M. B. Pepys, P. E. Fraser, *J. Mol. Biol.* **2000**, *300*, 1033–1039.
[66] J. L. Jiménez, E. J. Nettleton, M. Bouchard, C. V. Robinson, C. M. Dobson, H. R. Saibil, *Proc. Natl. Acad. Sci. USA* **2002**, *99*, 9196–9201.
[67] T. Theint, Y. Xia, P. S. Nadaud, D. Mukhopadhyay, C. D. Schwieters, K. Surewicz, W. K. Surewicz, C. P. Jaroniec, *J. Am. Chem. Soc.* **2018**, *140*, 13161–13166.
[68] D. Matthes, V. Daebel, K. Meyenberg, D. Riedel, G. Heim, U. Diederichsen, A. Lange, B. L. De Groot, *J. Mol. Biol.* **2014**, *426*, 362–376.
[69] S. Chen, V. Berthelier, J. B. Hamilton, B. O'Nuallain, R. Wetzel, *Biochemistry* **2002**, *41*, 7391–7399.
[70] C. Ma, J. Sun, B. Li, Y. Feng, Y. Sun, L. Xiang, B. Wu, L. Xiao, B. Liu, V. S. Petrovskii, Bin Liu, J. Zhang, Z. Wang, H. Li, L. Zhang, J. Li, F. Wang, R. Göstl, I. I. Potemkin, D. Chen, H. Zeng, H. Zhang, K. Liu, A. Herrmann, *Nat. Commun.* **2021**, *12*, 1–14.
[71] R. M. C. Vernon, P. A. Chong, B. Tsang, T. H. Kim, A. Bah, P. Farber, H. Lin, J. D. Forman-Kay, *eLife* **2018**, *7*, e31486.
[72] G. Kim, S. E. Lee, S. Jeong, J. Lee, D. Park, S. Chang, *Mol. Brain* **2021**, *14*, 1–11.
[73] K. Kamagata, R. Chiba, I. Kawahata, N. Iwaki, S. Kanbayashi, K. Maeda, H. Takahashi, A. Hirano, K. Fukunaga, K. Ikeda, T. Kameda, *Sci. Rep.* **2021**, *11*, 1–13.
[74] I. Bertini, C. Luchinat, G. Parigi, E. Ravera, B. Reif, P. Turano, *Proc. Natl. Acad. Sci. USA* **2011**, *108*, 10396–10399.
[75] C. Gardiennet, A. K. Schütz, A. Hunkeler, B. Kunert, L. Terradot, A. Böckmann, B. H. Meier, *Angew. Chem. Int. Ed.* **2012**, *51*, 7855–7858.
[76] T. Wiegand, D. Lacabanne, A. Torosyan, J. Boudet, R. Cadalbert, F. H. T. Allain, B. H. Meier, A. Böckmann, *Front. Mol. Biosci.* **2020**, *7*, 17.
[77] C. Gardiennet, T. Wiegand, A. Bazin, R. Cadalbert, B. Kunert, D. Lacabanne, I. Gutsche, L. Terradot, B. H. Meier, A. Böckmann, *J. Biomol. NMR* **2016**, *64*, 189–195.
[78] A. Böckmann, C. Gardiennet, R. Verel, A. Hunkeler, A. Loquet, G. Pintacuda, L. Emsley, B. H. Meier, A. Lesage, *J. Biomol. NMR* **2009**, *45*, 319–327.
[79] R. Fogh, J. Ionides, E. Ulrich, W. Boucher, W. Vranken, J. P. Linge, M. Habeck, W. Rieping, T. N. Bhat, J. Westbrook, K. Henrick, G. Gilliland, H. Berman, J. Thornton, M. Nilges, J. Markley, E. Laue, *Nat. Struct. Biol.* **2002**, *9*, 416–418.
[80] W. F. Vranken, W. Boucher, T. J. Stevens, R. H. Fogh, A. Pajon, M. Llinas, E. L. Ulrich, J. L. Markley, J. Ionides, E. D. Laue, *Proteins Struct. Funct. Genet.* **2005**, *59*, 687–696.
[81] T. J. Stevens, R. H. Fogh, W. Boucher, V. A. Higman, F. Eisenmenger, B. Bardiaux, B. J. Van Rossum, H. Oschkinat, E. D. Laue, *J. Biomol. NMR* **2011**, *51*, 437–447.
[82] M. D. Hanwell, D. E. Curtis, D. C. Lonie, T. Vandermeerschd, E. Zurek, G. R. Hutchison, *J. Cheminf.* **2012**, *4*, 1–17.
[83] D. Massiot, F. Fayon, M. Capron, I. King, S. Le Calvé, B. Alonso, J.-O. Durand, B. Bujoli, Z. Gan, G. Hoatson, *Magn. Reson. Chem.* **2002**, *40*, 70–76.
[84] S. Hediger, B. H. Meier, R. R. Ernst, *Chem. Phys. Lett.* **1995**, *240*, 449–456.

Manuscript received: April 12, 2023
Accepted manuscript online: June 13, 2023
Version of record online: August 7, 2023